Detection of defects in a transparent polymer with high resolution tomography using white light scanning interferometry and noise reduction

A. Leong-Hoï[a*], R. Claveau[a], M. Flury[a], W. Uhring[a], B. Serio[b], F. Anstotz[a] and P. C. Montgomery[a]

[a] Laboratoire des Sciences de l'Ingénieur, de l'Informatique et de l'Imagerie (ICube), UDS-CNRS, UMR 7357, 300 bd Sébastien Brant, CS 10413, F-67412 Illkirch cedex, France

[b] Laboratoire Energétique Mécanique Electromagnétisme (LEME) - EA 4416, 50 rue de Sèvres, 92410 Ville d'Avray, France

ABSTRACT

Transparent layers such as polymers are complex and can contain defects which are not detectable with classical optical inspection techniques. With an interference microscope, tomographic analysis can be used to obtain initial structural information over the depth of the sample by scanning the fringes along the Z axis and performing appropriate signal processing to extract the fringe envelope. By observing the resulting XZ section, low contrast, sub-µm sized defects can be lost in the noise which is present in images acquired with a CCD camera. It is possible to reduce temporal and spatial noise from the camera by applying image processing methods such as image averaging, dark frame subtraction or flat field division. In this paper, we present some first results obtained by this means with a white light scanning interferometer on a Mylar polymer, used currently as an insulator in electronics and micro-electronics. We show that sub-µm sized structures contained in the layer, initially lost in noise and barely observable, can be detected by applying a combination of image processing methods to each of the scanned XY images along the Z-axis. In addition, errors from optical imperfections such as dust particles on the lenses or components of the system can be compensated for with this method. We thus demonstrate that XZ section images of a transparent sample can be denoised by improving each of the XY acquisition images. A quantitative study of the noise reduction is presented in order to validate the performance of this technique.

Keywords: High resolution tomography, white light scanning interferometry, transparent polymer, defect detection, XY-XZ image processing, noise reduction.

*aleonghoi@unistra.fr; phone (+33) 3 68 85 46 27; icube-ipp.unistra.fr

1. INTRODUCTION

Transparent layers such as polymers are complex and can contain defects which are not detectable with classical optical inspection techniques. In the µm to sub-µm resolution range, several techniques exist to perform accurate measurement, such as confocal microscopy[1] or interference microscopy[2].

White light scanning interferometry (WLSI), or coherence scanning interferometry (CSI) is a measurement method based on the acquisition of an image sequence of interference patterns resulting from the superposition of the light from the object to be measured and the light reflected from a reference mirror[3–5]. Interference fringes appear in the image plane of the optical system in which a video camera is placed. For surface roughness measurement, a variation along the optical axis between the objective and sample is introduced, for example using a piezoelectric scanner, to record the change in light intensity resulting from interference. But in the case of imaging interfaces and structures buried under transparent layers[6,7], the fringe signal suffers from degradation due to several factors, such as noise and artifacts. Indeed, with an interference microscope, tomographic analysis can be used to obtain initial structural information over the depth of the sample by scanning the fringes along the Z axis and performing appropriate signal processing to extract the fringe envelope[8]. By observing the resulting XZ section, sub-µm sized defects can be lost in the noise which is present in images acquired with a CCD camera.

A CCD camera is composed of a matrix of pixels which transform the incident photons into electrons. These electrons are read by the electronic system and are converted into a digital value representing intensity in gray levels of the image[9]. However, acquired images are noisy. There are several image degradation sources due to the camera[10]. One of them is the random noise, also called readout noise, of the camera which varies with time and can be reduced by image averaging. Another degradation source is the "fixed pattern noise" (FPN)[11,12]. The default value of each pixel without light is not uniform along the entire sensor array. This problem meanly arises from small differences in the pixel, such as the pixel area mismatch in a CCD sensor and the offset of the pixel amplifier in a CMOS sensor. These effects can be corrected by subtracting the image by the dark image obtained by obstructing the illumination path. In addition, the background illumination intensity can also itself be a source of noise in images because of the non-homogeneous illumination on the sample. Moreover, the CCD camera also suffers from a photo response non-uniformity, called the PRNU, which is a mismatch in the pixel gain. One way of compensating this is to divide the image by the so-called "flat field" image[13]. This operation makes it possible to overcome the vignetting problem and to remove eventual details due to dust particles on the lenses or components of the system. Temporal noise is also present while the images are acquired, which can be removed by simple image averaging[14]. It is thus possible to reduce temporal and spatial noise from the camera by applying such image processing methods[15].

In this paper, we present some initial results obtained by this means with a white light scanning interferometer on a Mylar polymer of 3.6 μm thickness, an important material used currently as an insulator in electronics and micro-electronics. The system is an adapted Leitz-Linnik interferometric microscope with x50 objectives (NA = 0.85) and a CCD camera[6,7]. We show that structures of about 1.2 μm in size contained in the layer, initially lost in noise and barely observable, can be detected by applying a combination of image processing methods to each of the scanned XY images along the Z-axis. In addition, errors from optical imperfections such as those due to dust particles on the lenses or components of the system can be compensated for with this method and reduced in size to about 1 μm. We thus demonstrate that XZ section images of a transparent sample can be denoised by improving each of the XY acquisition images. The technique of noise reduction leads to an improvement in the axial detection sensitivity of internal details in the tomographic section of transparent layers. A quantitative study of the noise reduction is presented in order to validate the performance of this technique. Image averaging increases the stability of the acquisitions by reducing temporal noise, while dark frame and flat field corrections are involved in the spatial noise reduction of images. The last two corrections allow a lateral resolution improvement of up to 140 nm.

2. THEORETICAL BACKGROUND

2.1 XZ image processing from XYZ image stack

Optical interference microscopy makes use of a series of white light fringes superimposed on the image of the sample. These fringes are scanned over the whole depth of the sample by changing the distance between the objective and the sample surface using a piezoelectric device[5,6]. At each displacement of the piezoelectric translator, an XY image is acquired with the camera, leading to a stack of XYZ images, as illustrated in the example in Figure 1(a). The fringe signals along the optical axis at each pixel in an image are processed in order to determine the fringe envelope, where the different peaks indicate the positions of certain features (interfaces, structures…) within the sample, as shown in Figure 1(b). In monochromatic light, for a given pixel (x,y) in an XY image, the intensity I(z) at the detector as a function of the position along the optical axis z can be written:

$$I(z) = I_0\big[1 + \gamma(z).\cos\big(\phi(z)\big)\big]$$ (1)

where I_0 is a constant related to the intensity of the source, $\gamma(z)$ is the fringe visibility, or fringe contrast, and $\phi(z)$ is the phase term. In the case of white light illumination (polychromatic case), only the rays of the same wavelength can interfere with each other, so the total intensity is the sum of the interferences at each wavelength :

$$I(z) = \int_{\lambda_1}^{\lambda_2} I_0(\lambda).\big[1 + \gamma(z).\cos\big(\phi(\lambda, z)\big)\big]\, d\lambda$$ (2)

where (λ_1, λ_2) define the spectral bandwidth of the illumination source, $I_0(\lambda)$ is a function that takes into account the spectral distribution and intensity of the illumination source and the spectral responses of the components within the

optical system, $\gamma(z)$ is the fringe visibility depending on some optical system parameters such as the numerical aperture of the objective and $\phi(\lambda, z)$ is the phase linked to the optical path difference between the two waves that interfere that takes into account the difference in nature between the reference mirror and the sample.

By rotating the XYZ image stack, XZ images can be extracted in which the interference fringes along the Z axis are observable, as shown in Figure 1(c). Using the 2D fringe processing[8], results in new XZ images show the fringe envelopes, as illustrated in Figure 1(d). In these tomographic images, surfaces and other structures within the transparent sample are then perceptible. Although the 2D approach is satisfactory, it is not sufficient for the detection of smaller details that are lost in the noise (in the circle in Figure 1(d)).
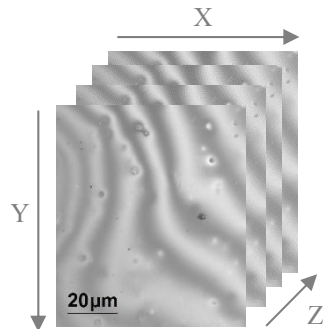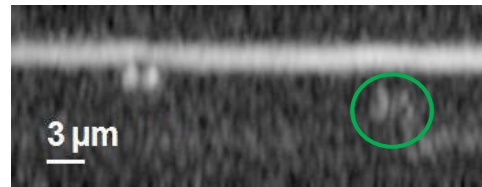

(a) Stack of XYZ images.
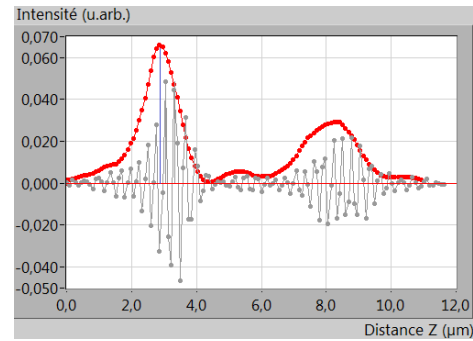
(b) Fringe signals from a pixel in an XY image from the XYZ image stack.
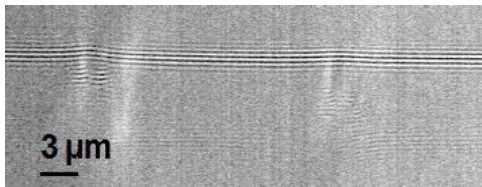
(c) Raw fringes in an XZ image from the XYZ image stack.

(d) Processed fringes from (c) using 2D processing, shown with a log scale.

Figure 1. Example of an image stack XYZ, 1D fringe signal processing from a pixel in an XY image and 2D fringe signal processing on a 3.6 μm thick Mylar film.

2.2 Temporal and spatial image corrections

Two types of noise can be distinguished when an image is acquired with a CCD camera. The readout noise, is a temporal noise which can be considered as random fluctuations which vary over time. Consequently, the grayscales of the same pixels in two acquisitions taken at different times will display small variations. In the case of a static sample, this temporal noise can be reduced by averaging several consecutive images, with the noise reduction being proportional to the square root of the number of images used. The equation for the image averaging I_{moy} is given by:

$$I_{moy} = \frac{1}{N} \sum_{i=1}^{N} I_i$$

(3)

where N is the number of images and I_i is the ith image with $i = \{1, \dots, N\}$.

The second type of noise is spatial. This noise can come from the fixed pattern noise which is characterized by more or less bright pixels which appear in the same positon in the images when they are acquired in the same circumstances. The FPN can be corrected by subtracting the images by the dark image, as shown by Eq. (4).

$$I_{corrDark} = I - I_{Dark}$$

(4)

I_{Dark} is the dark image obtained by obstructing the illumination path. In addition, the spatial noise can also come from the photo response non uniformity of the camera, the PRNU, or from the non-homogeneous background illumination which can contain projections of dust particles or dirt present on the optical components of the system. A way of compensating this is to divide the image by the so-called "Flat field" image:

$$I_{corrFlat} = \frac{I}{I_{Flat}} * C \qquad (5)$$

where C is a constant between 0 and 255, in the case of a 8-bit resolution camera, which can be equal to the mean value of the flat field image.

In this paper, we propose an image correction, given by Eq. (6) which combines these three image processing techniques:

$$I_{corrected} = \frac{I_{moy} - I_{Dark}}{I_{Flat} - I_{Dark}} * C \qquad (6)$$

3. EXPERIMENTAL SETUP

3.1 Microscope system

The system developed to carry out the experiment is an adapted Leitz-Linnik interference microscope composed of x50 objectives (NA = 0.85). The image acquisition is performed with a Basler avA1000-100gc GigE CCD camera having 1024x1024 pixels and a Giga Ethernet connection. The sample is mounted on a piezoelectric table (PIFOC, from PI) for Z-scanning (Figure 2). The piezo actuator is controlled in a closed loop with a capacitive position sensor, having a position sensitivity of 1 nm. Acquisition and processing is carried out on a PC equipped with an Intel® Xeon® CPU processor (2.40 GHz, 8 Go RAM) with a Windows 7 (64 bits) operating system.
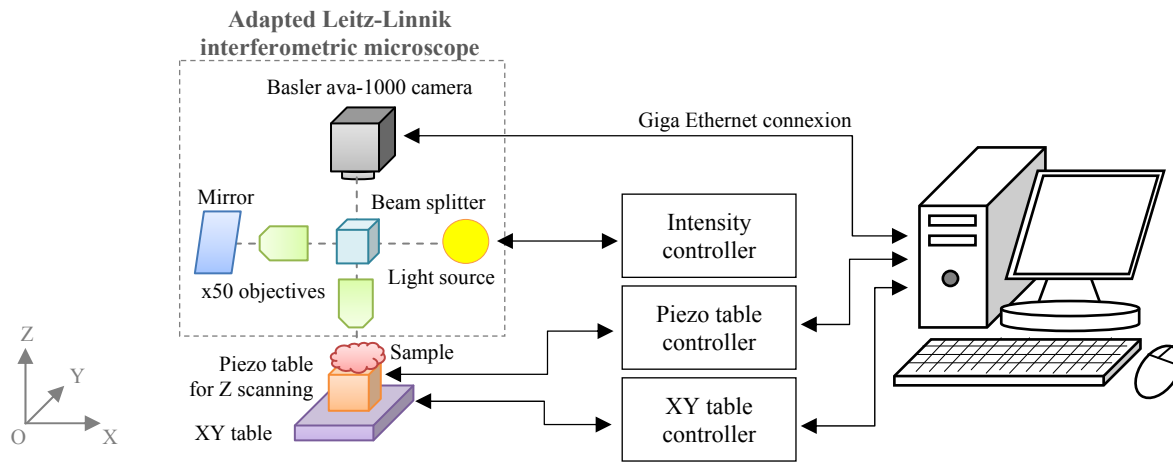

Figure 2. Schematic layout of the interference microscopy system.

3.2 Software implementation

The software used to control the system is written in LabVIEW (version 2014, 64 bits, NI). For the acquisition, image processing and measurements, a program was developed using the IMAQ Vision module. The global layout for the signal and image acquisition and processing is given in Figure 3. The first step is to build up a XYZ image stack by performing a fast acquisition of XY images while scanning over the depth of the sample[8]. These images are stored on hard disc and then loaded into RAM memory for performing the required post processing and analysis. The type of tomographic analysis required can be chosen by rotating the computed stack and observing the XZ images at different planes in Y or just to display the XY images as a function of Z and then observe the fringe signal along the Z axis at different pixels using the Z-scan technique.

The technique developed previously[8] allowed the building up of an XYZ image stack with only one acquisition at each vertical displacement of the piezoelectric device. The results obtained on the XZ images enable the observation of the rear and front sides of a transparent layer. However, the high presence of noise in the XZ sections prevents the detection of micrometric structures within the sample (Figure 1(d)).

In order to reduce the noise, the technique was improved to include the different image corrections presented in section 2.2. An option was then added to allow the recording at each Z position of an image obtained either with one acquisition or after an averaging of N images. To apply the dark and flat corrections, it is necessary to acquire the dark and flat images by taking care to be in the same measurement conditions (light source intensity, camera parameters: gain, exposure time…).

The dark image is obtained by obstructing the illumination path of the system. The flat image corresponds to the defocused image of a white homogenous sample placed below the objective. For a better correction it is possible to use averaging for each of the dark and flat images.
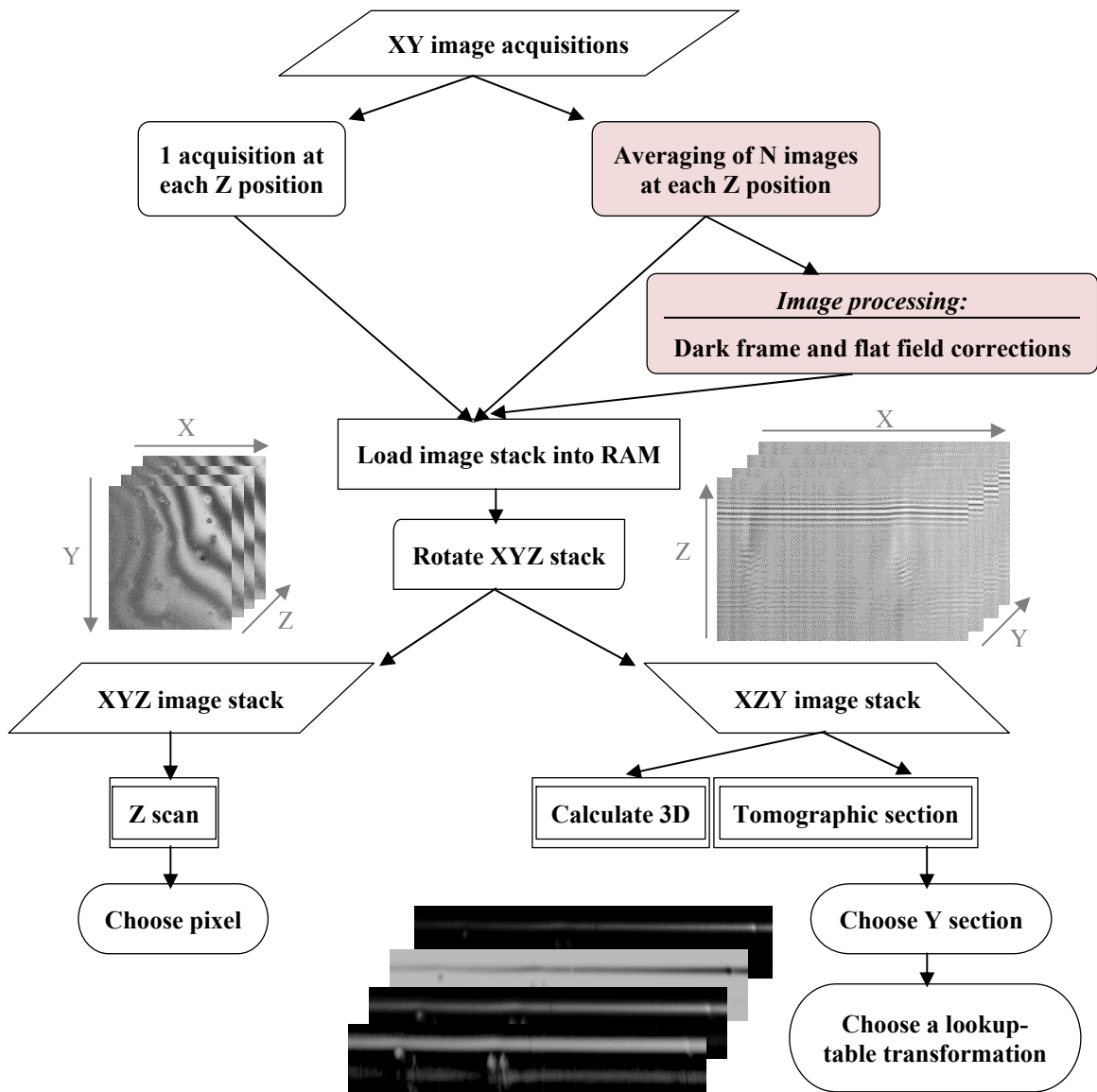

Figure 3. Flow chart of fringe signal processing.

A lookup-table transformation is then performed by remapping the pixel values in the image. A Lookup table is a grayscale replacement table containing a maximum of 256 elements for an 8-bit image. If we note T_i the ith coefficient of the initial lookup-table:

$$T_i = 0, 1, 2, ..., I_{max} - 1 = i \qquad (7)$$

with $I_{max} \leq 256$. The details in Figure 4 indicate the equations associated to each transformation and an example of an XZ image of the Mylar sample. We note that with a linear transformation the front side of the layer is observable and a small structure appears (in the square). With the inverse transformation, another structure can hardly be observed (in the circle). The square root transformation improves the detection of defects but has a drawback of increasing the noise. With a logarithmic transformation small structures can be better measured but the noise also increases. For the subsequent results, the XZ images with a logarithmic transformation are shown in order to underline the improvement of the SNR of the images after the proposed corrections.
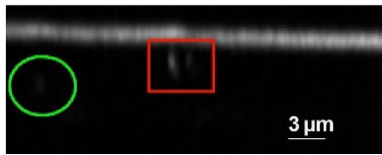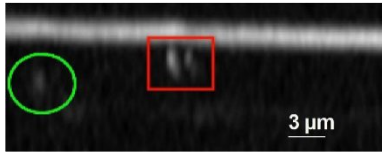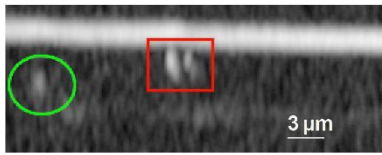
Transformation	Associated equation	Example of XZ image
Linear	$T_i^{linear} = T_i$	
Inverse	$T_i^{inverse} = I_{max} - i$	
Square root	$T_i^{sq\ root} = \dfrac{\sqrt{i} * I_{max}}{\sqrt{I_{max}}}$	
Logarithm	$T_i^{log} = \dfrac{Log(i+1) * (I_{max} - 1)}{Log(I_{max} - 1)}$	

Figure 4. Lookup-table transformations for XZ images.

3.3 **Noise analysis**

To understand the consequences of the proposed image processing on a simple image, a study of noise quantification has been carried out.
Image averaging allows a decrease in the temporal noise. To quantify this reduction between a simple image and an averaged image, M acquisitions are taken for both methods and the signal-to-noise ratios (SNR) in dB on the same pixel x are compared, as shown in Eq. (8).

$$SNR_{dB} = 10 * \log\left(\frac{\bar{x}}{\sigma}\right) \qquad (8)$$

where $\bar{x} = \sum_{i=1}^{M} x_i$ is the mean value of the same pixel of the M acquired images and $\sigma = \sqrt{\frac{1}{M}\sum_{i=1}^{M}(x_i - \bar{x})^2}$ is the standard deviation. The results in Figure 5 show the SNR, as given in Eq. (8) of the pixel at position (x = 10 ; y = 233) for 10 images averaged N times, with N varying between 1 and 100. This underlines that the SNR is enhanced by a factor of $\sqrt{N}$, with N being the number of images. These results reveal that averaging between 20 and 50 images is sufficient for an adequate SNR.

For the dark frame correction, the image improvement is not visible in the image but can be calculated with the root mean square (RMS) value R_q of the dark frame as follows:

$$R_q = \sqrt{\frac{1}{p}\sum_{i=1}^{p} x_i{}^2}$$

(9)

with p is the total number of pixels and x_i is the ith pixel of the image.
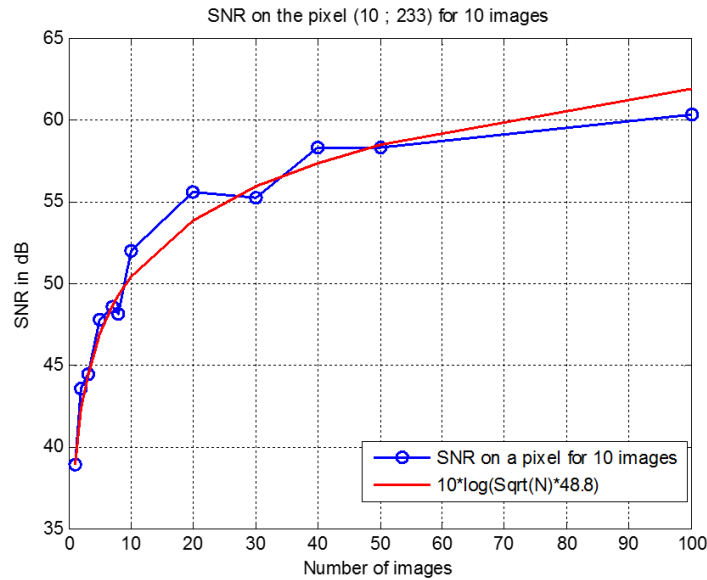

Figure 5. Signal to Noise Ratio of the pixel at position (10 ; 233) for 10 images of images averaged N times.

Before performing the dark correction, an averaging of the dark frames can be carried out. Table 1 indicates the pixel values obtained after dark frame averaging. The pixel values vary between 1 and 7 gray levels. With a high number of images the standard deviation of the pixel intensities slowly decreases. The histograms obtained for an averaging of 20 images and 100 images are almost the same, as shown in Figure 6. This indicates that the FPN is well caracterized with only 20 averaged frames.

Table 1. Pixel values for the dark frame averaged 20x and 100x.

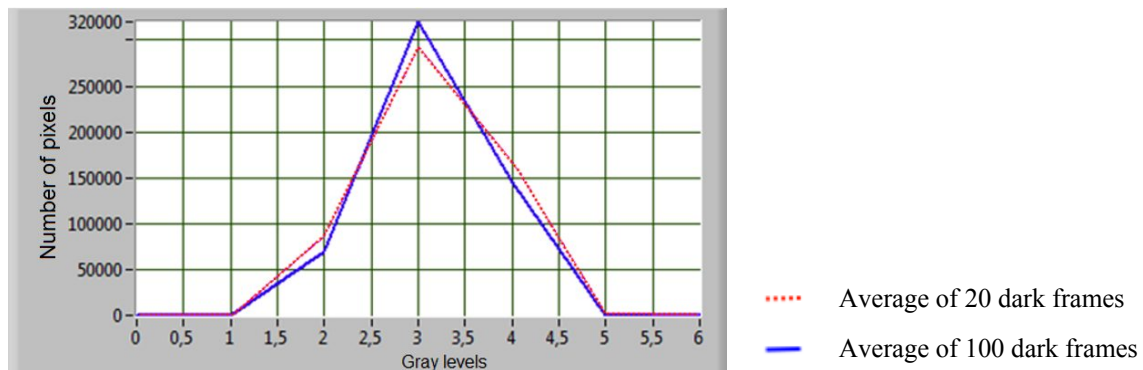|	Min*	Max*	Mean*	Standard deviation*	RMS*
Average of 20 dark frames	1	7	3.16	0.68	3.23
Average of 100 dark frames	1	7	3.14	0.62	3.20

*(in gray levels)

Figure 6. Histograms of a dark frame averaged 20x and 100x.

In Figure 7, the histogram of an image averaged 100 times is compared to the same after applying the dark correction. The Full width at half maximum (FWHM) of the histogram after the dark subtraction is better by 3 gray levels than without the dark correction (Table 2).

Table 2. Full width at half maximum for an image averaged 100x and the same image after subtracting the dark image.

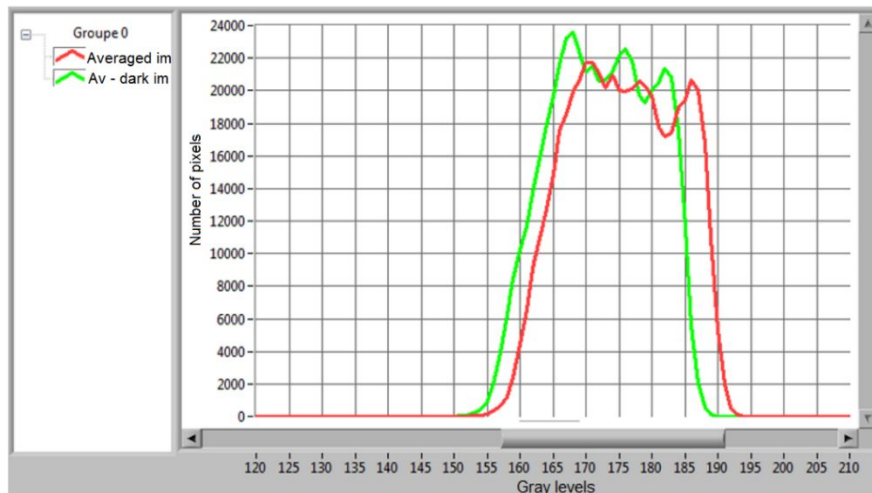|	Averaged 100x	Averaged 100x - Dark
FWHM (in gray levels)	26	23

Figure 7. Histograms of an image averaged 100x and the same image after subtracting the dark image.

For the flat field correction, the histograms of a uniform image are observed, as shown in Figure 8. If the histogram is narrower and looks like a Dirac function, then the image is improved. The results of the values of FWHM in Table 3 highlight that the histogram is almost 10 times narrower after the dark and flat corrections than for a raw image acquisition.

Table 3. Full width at half maximum for the histograms obtained with the 4 methods.

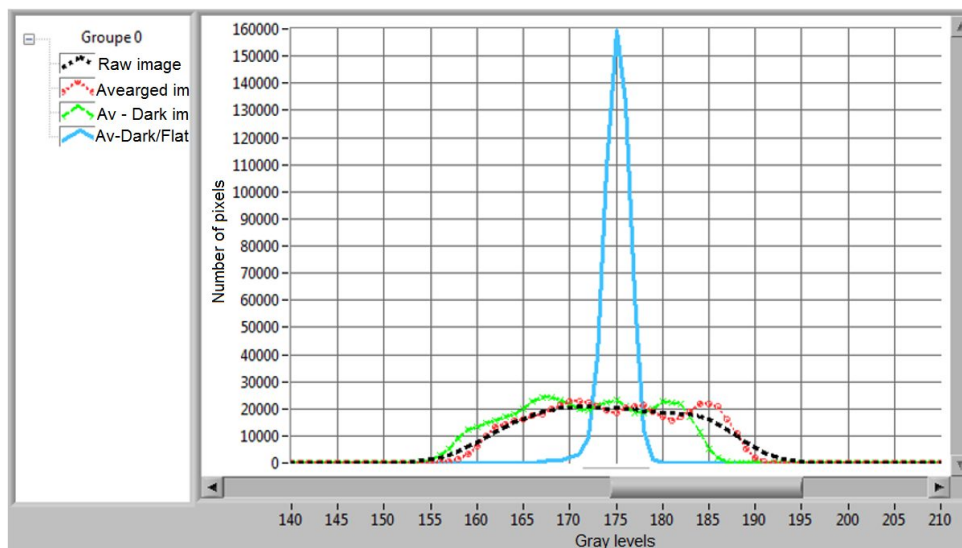|	Raw im.	Averaged 100x	Averaged 100x - Dark	(Averaged 100x – Dark) /(Flat-Dark)
FWHM (in gray levels)	28	26	24	3

Figure 8. Histograms of a flat image for the 4 methods.

4. RESULTS

In all the results that follow, the dark frame and the flat image used consist of averages of 20 dark frames and 20 flat images, for the Mylar polymer film of 3.6 μm thickness.

4.1 Detection of structures

Image averaging thus allows an improvement in the signal to noise ratio for the XY and XZ images and so leads to the observation of μm-sized structures, initially lost in the noise. At one position, as shown in Figure 9(a), a defect can be distinguished in Figure 9(b) (arrow). After an average of 10 XY images for each vertical position of the piezoelectric table, the previous defect remains observable as illustrated in Figure 9(c) (arrow), and a structure of about 3 μm appears (in the circle) whereas it was not visible without correction in Figure 9(b) (in the circle).

(a) Position of the cross section on the XY image.

(b) XZ image without correction.

(c) XZ image after averaging 10x.
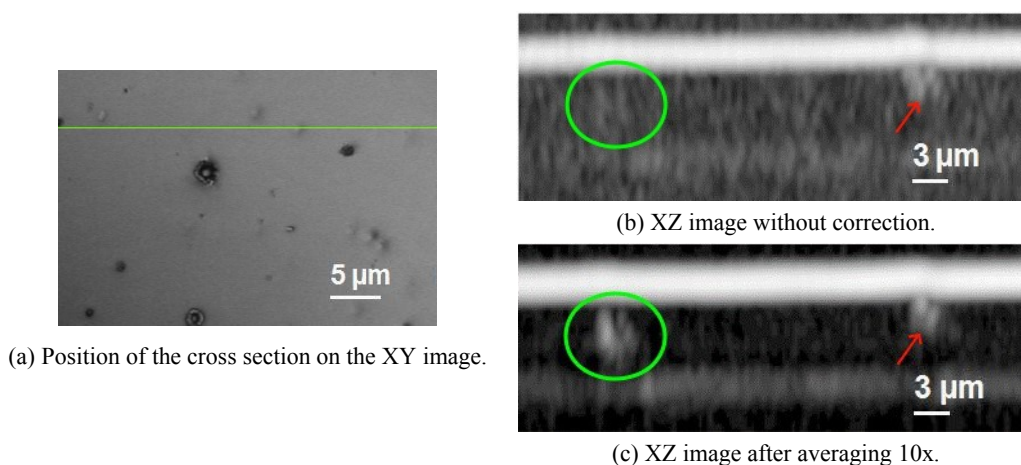
Figure 9. Detection of a 3 μm sized structure after averaging 10x.

However, sometimes averaging 10 times is not enough to detect smaller structures. In Figure 10, a 1.75 μm sized structure is barely visible (in the circle) after averaging 10 times, as shown in Figure 10(b), whereas it is observable and measurable after averaging 50 times, as illustrated in Figure 10(c). This improvement is due to the fact that after averaging 10 times, the noise is reduced by a factor of 3, while after averaging 50 times, the noise is reduced by a factor of 7 (i.e. twice as better). For the subsequent work, averaging of 100 XY images for each Z position is used, which corresponds to a reduction of the noise by a factor of 10.
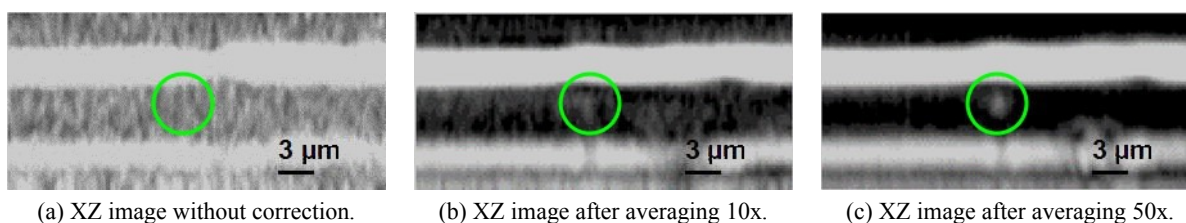

(a) XZ image without correction.   (b) XZ image after averaging 10x.   (c) XZ image after averaging 50x.

Figure 10. Detection of a 1.75 μm sized structure after averaging 50x.

4.2 Improvement in the lateral resolution

Each optical system has a limit of resolution (~ 400 nm for visible light microscopy), but in practice on account of certain factors such as the noise due to the camera or the effects of diffraction, this optical resolution is not easily achieved. The proposed method for combining image processing techniques allows an improvement in the lateral resolution of the acquired images by removing certain noise contributions so as to better approach the theoretical optical resolution limit of the system.

An improvement in lateral resolution is obtained by using dark and flat corrections after averaging 100 XY images. Figures 11(a) and 11(c) represent respectively the XZ images after averaging 100x and after the corrections given by Eq. (6) with I_{moy} images averaged 100 times and $C = 120$, in which the position of a cross section of a pore type defect is displayed. Figures 11(b) and 11(d) show the respective line profiles. The measurements of the size of the structure reveal that the dark and flat corrections for this sample have allowed a lateral resolution improvement of 70 nm. The axial resolution is not always improved.
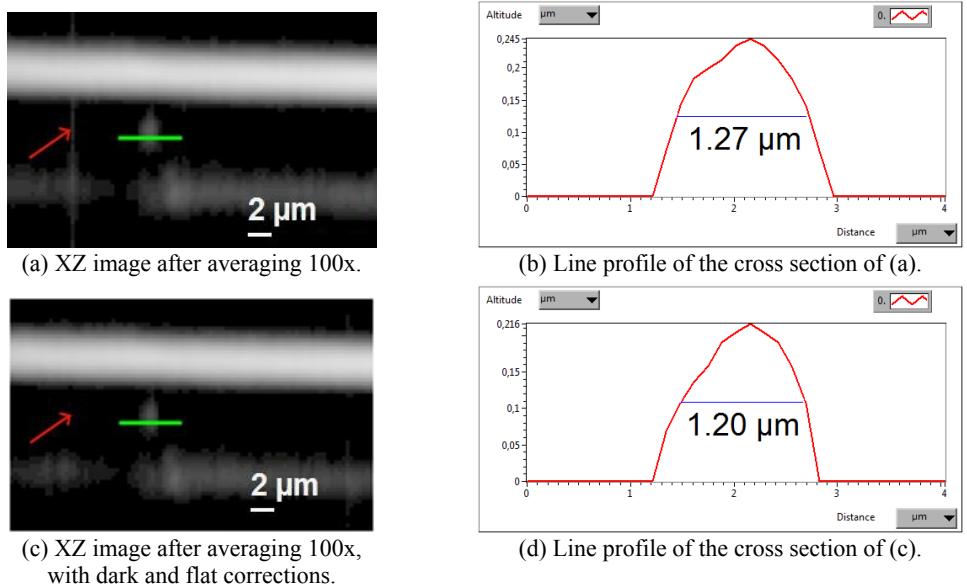

(a) XZ image after averaging 100x.

(b) Line profile of the cross section of (a).

(c) XZ image after averaging 100x, with dark and flat corrections.

(d) Line profile of the cross section of (c).

Figure 11. Improvement of the lateral resolution after dark and flat corrections.

4.3 Reduction of unwanted optical defects

The optical components of a system are not always perfect and some defects, such as dust particles or grease can be present. Sometimes, they are not easily noticeable or it is not convenient to remove the optical components in order to clean them. The dark and flat corrections have the advantage of reducing or even removing these unwanted image defects. In Figure 11(a), an image defect from the optical system (arrow) has been removed after correction, as shown in Figure 11(c). In addition, while a structure remains visible (arrow) together after simply averaging 100 times and after the corrections given by Eq. (6) with I_{moy} images averaged 100 times and $C = 120$, in Figure 12(b) and 12(c) respectively, another defect (in the square) has been removed after dark and flat corrections in Figure 12(c). This 1.5 µm sized defect is also observable in the flat image in Figure 12(a). Its presence in this image proves that it concerns a dust particle on an optical component of the system. A comparison of the line profiles of the intensity of the image defect shown in Figure 13(d) provides more convincing proof.
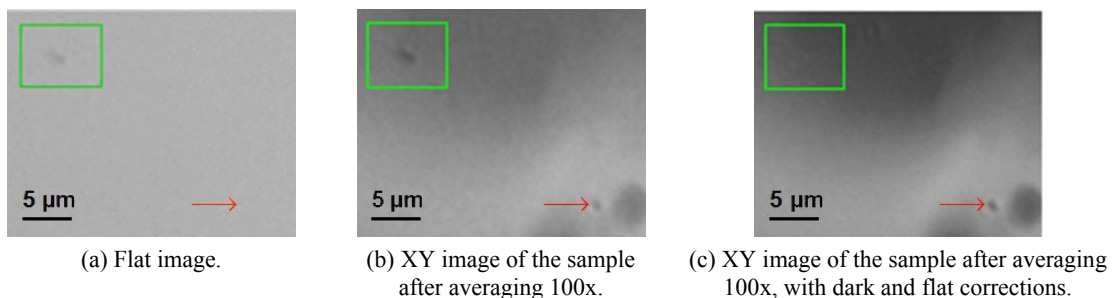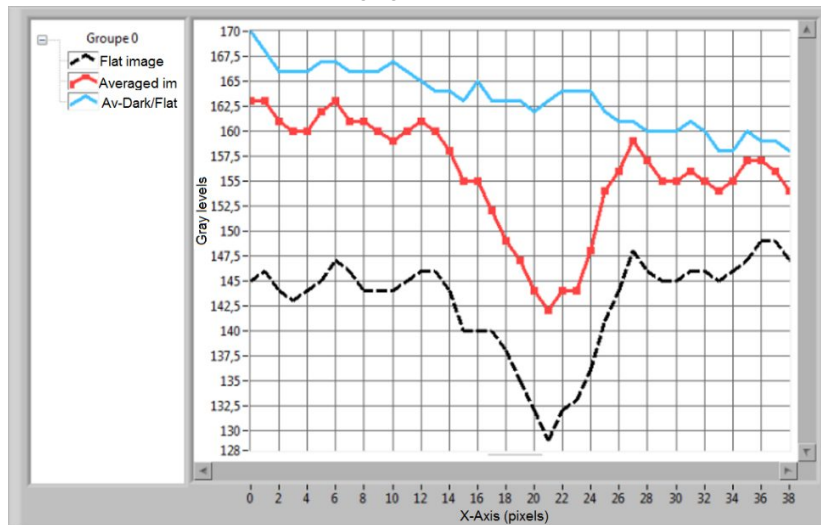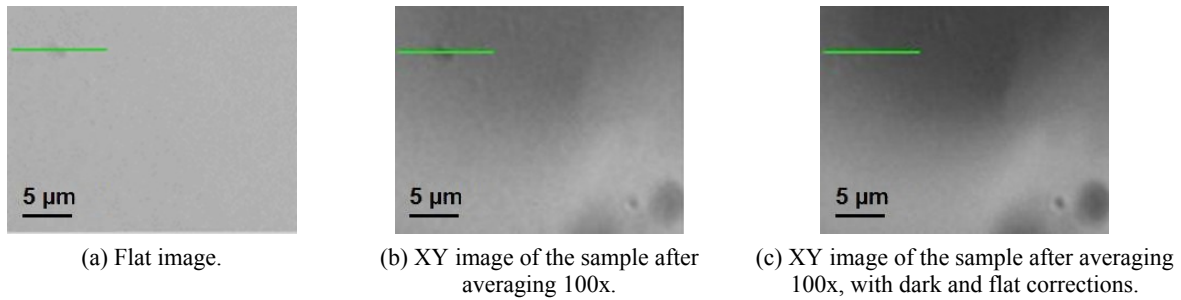

(a) Flat image.

(b) XY image of the sample after averaging 100x.

(c) XY image of the sample after averaging 100x, with dark and flat corrections.

Figure 12. Removal of a dust particle of 1.5 µm after dark and flat corrections.

(a) Flat image.

(b) XY image of the sample after averaging 100x.

(c) XY image of the sample after averaging 100x, with dark and flat corrections.

(d) Cross sections of the images (a), (b) and (c).

Figure 13. Cross sections of a dust particle.

While some unwanted image defects can be too significant to be totally removed, they can be greatly reduced with dark and flat corrections. For the defect illustrated in Figures 14(a) and 14(c), the structure has been reduced in diameter by about 0.8 µm after dark and flat corrections. Although the defects in Figures 13 and 14 have the same lateral size (about 1.8 µm), the difference in the gray levels compared to the mean of the intensity of the pixels in the flat image is lower for the defect in Figure 13 (19 gray levels) than that in Figure 14 (76 gray levels). This could be the reason why the defect in the first one has been totally removed whereas the second one has just been reduced.
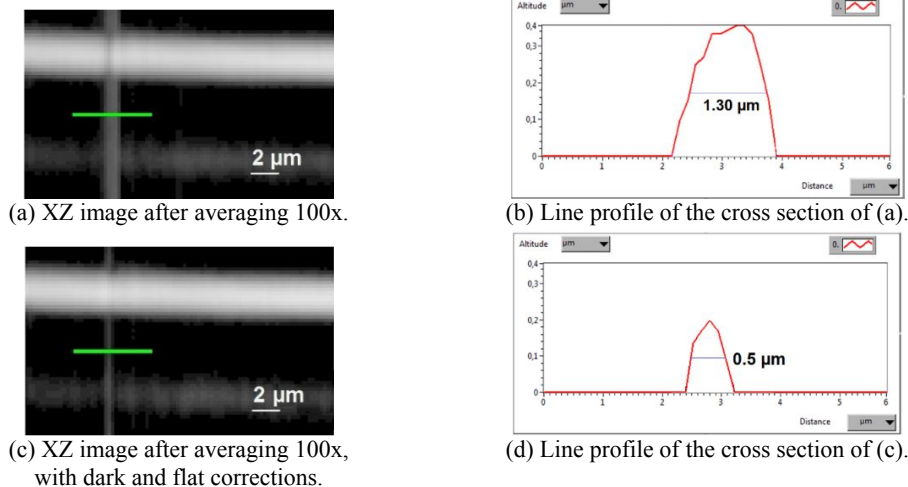
(a) XZ image after averaging 100x.

(b) Line profile of the cross section of (a).

(c) XZ image after averaging 100x, with dark and flat corrections.

(d) Line profile of the cross section of (c).

Figure 14. Reduction of a dust particle after dark and flat corrections.

5. CONCLUSION

In this paper, we have presented the application of white light scanning interferometry assisted with carefully chosen image processing techniques to improve the performance in characterizing the internal structural defects of a transparent polymer film. The method proposed allows the imaging of structures of about 1.5 µm in diameter contained within the layer, initially lost in noise and barely observable. The technique is based on the acquisition of a stack of XY images followed by different image corrections to reduce the noise. A rotation is then carried out on the XYZ images to obtain XZX images. A 2D processing of the fringes in the XZ plane is then performed to improve again the robustness to noise. Among the image processing methods used, image averaging increases the stability of the acquisitions by reducing temporal noise, while dark frame, obtained by obstructing the illumination path of the optical system, and flat field corrections are involved in the spatial noise reduction of the images. The last two corrections allow a lateral resolution improvement of at least 100 nm. A quantitative study of the noise reduction has been presented in order to validate the performance of this technique and to quantify the SNR improvement of the images. The result is an improvement in the detection sensitivity of internal details in the tomographic section of transparent layers. In addition, the practical lateral resolution of the images acquired with the optical system is improved and errors from optical imperfections such as dust particles on the lenses or components of the system can be compensated for with this method and reduced in size by nearly 1 µm.

ACKNOWLEDGMENTS

REFERENCES

[1]   Shotton, D. M., "Confocal scanning optical microscopy and its applications for biological specimens," J. Cell Sci. **94**(2), 175–206 (1989).

[2]   Montgomery, P., Anstotz, F., Johnson, G.., Kiefer, R., "Real time surface morphology analysis of semiconductor materials and devices using 4D interference microscopy," J. Mater. Sci. Mater. Electron. **19**(1), 194–198 (2008).

[3]   Coupland, J. M.., Lobera, J., "Measurement of Steep Surfaces Using White Light Interferometry," Strain **46**(1), 69–78 (2010).

[4]   Montgomery, P. C., Montaner, D., Manzardo, O., Flury, M.., Herzig, H. P., "The metrology of a miniature FT spectrometer MOEMS device using white light scanning interference microscopy," Thin Solid Films **450**(1), 79–83 (2004).

[5]   Pecheva, E., Montgomery, P., Montaner, D.., Pramatarova, L., "White Light Scanning Interferometry Adapted for Large-Area Optical Analysis of Thick and Rough Hydroxyapatite Layers," Langmuir **23**(7), 3912–3918 (2007).

[6]   Benatmane, A.., Montgomery, P. C., "3D analysis of buried interfaces using interference microscopy," Eur. Phys. J. Appl. Phys. **27**(1-3), 411–414 (2004).

[7]   Benhaddou, D., Montgomery, P. C., Montaner, D.., Bonnafé, J., "Buried interface characterization in optoelectronic materials by interference microscopy," J. Mod. Opt. **48**(3), 533–547 (2001).

[8]   Montgomery, P. C., Montaner, D.., Salzenstein, F., "Tomographic analysis of medium thickness transparent layers using white light scanning interferometry and XZ fringe image processing," Proc. SPIE **8430**, 843014–843014 – 9 (2012).

[9]   Mullikin, J. C., van Vliet, L. J., Netten, H., Boddeke, F. R., van der Feltz, G.., Young, I. T., "Methods for CCD camera characterization," Proc. SPIE **2173**, 73–84 (1994).

[10] Healey, G. E.., Kondepudy, R., "Radiometric CCD camera calibration and noise estimation," IEEE Trans. Pattern Anal. Mach. Intell. **16**(3), 267–276 (1994).

[11] Lukas, J., Fridrich, J.., Goljan, M., "Digital camera identification from sensor pattern noise," IEEE Trans. Inf. Forensics Secur. **1**(2), 205–214 (2006).

[12] Michel, R., Fordham, J.., Kawakami, H., "Fixed pattern noise in high-resolution, CCD readout photon-counting detectors," Mon. Not. R. Astron. Soc. **292**(3), 611–620 (1997).

[13] Seibert, J. A., Boone, J. M.., Lindfors, K. K., "Flat-field correction technique for digital detectors," Proc. SPIE **3336**, 348–354 (1998).

[14] Petrou, M.., Petrou, C., [Image Processing: The Fundamentals], John Wiley & Sons, Chichester, 880 (2010).

[15] Russ, J. C., [The image processing handbook, 3rd ed], CRC Press, Boca Raton, Florida, 771 (1998).